Article

Novel arrangement for pin-fin heat sinks for improves the optimization of thermal dissipation

Juan Ramirez-Vazquez[1] and Martin Nieto-Perez[2]

[1]CICATA Querétaro, Instituto Politecnico Nacional, Cerro Blanco 141, 76090, Colinas del Cimatario, Santiago de Querétaro, México, jpramvaz@gmail.com

[2]CICATA Querétaro, Instituto Politecnico Nacional, Cerro Blanco 141, 76090, Colinas del Cimatario, Santiago de Querétaro, México, mnieto@psu.edu

*jpramvaz@gmail.com, +52 442 604 6685

Abstract: This work presents a design and model of the thermo-hydrodynamic behavior applying CFD for pin-fin heat sink with square shape (rectangular fin profile), through a novel pin arrangement that improves heat removal in the system. The novelty consist in the insertion of a deflector row that will help to direct the flow, so it hits the rectangular cross-sectional fins the presents in the system. The heat sink model is placed in channel designed in which air flows as suitable medium, and its overall performance is investigated. In addition, a constant heat flux is applied to the bottom wall of the heat sink model, equal values and amounts that correspond to the heat fluxes generated by current electronic equipment and devices. The numerical results of the global thermal resistance, the pressure drop and the Nusselt number are reported. The results allow determining best arrangement or geometry configuration, location and functionality of the fin-deflectors were collocated for evaluate thermal-hydraulic efficiency of system.

Keywords: Heat sinks; Global thermal resistance; Pressure drop; Nusselt number; Fin- deflectors; Computational Fluid Dynamics (CFD)

1. Introduction

The document consists of seven sections, the first is presented as an introduction which begins by describing the problem in study questions, is contrasted with the related works and a solution is proposed that partially or totally pays the problem. Sequentially, in the second sections is reviewed the description of the problem. In the third, fourth, fifth the experiments configuration carried out are described respectively; as well as the results in the sixth section are presented following a logical sequence in the text, tables and specific figures interpreted, highlighting first the most important findings, in order and consistent with the research objectives. Finally, in the seventh section, the most conclusions innovative and important aspect are detailed.

1.1. Background

The power devices have gained significance in actual years as they provide numerous environmental, economic, and national interest benefits over the conventional internal combustion engine-based vehicles [1-3]. Electronic equipment operating in thermal hostile environment demand special care in thermal sizing at the design stage, fixing attention on power losses minimization and cooling system optimization [4].

The study was conducted and suggested as a result of the urgent need previous featured [5], for explaining the behavior of heat sinks as elements that dissipate the heat generated by devices electronic. Proper heat sink design has been shown to improve efficiency and extend the life of electronic devices in use. Therefore, heat sinks must be designed and constructed to be reliable, efficient, and economical.

Over the past 20 years, research into heat sinks in computer equipment has made great strides both experimentally and numerically. Ahmed et al. [6] performed a comprehensive review of how

Preprints (www.preprints.org) | NOT PEER-REVIEWED | Posted: 6 June 2023 doi:10.20944/preprints202306.0457.v1

to optimize the thermal fluid design of heat sinks. To do this, they examined available research on active and passive techniques used to improve heat sink energy dissipation by modifying either the solid or liquid domain. On the other hand, Ayub et al. [7] conducted an experimental analysis to generate a larger heat transfer area. To do this, we tested several copper heat sinks with different distances between the fins, as shown in Figure 1. During the experiment, they found a very low temperature on the underside of the processor, a temperature of 0.5°Cat 325W of heat output.

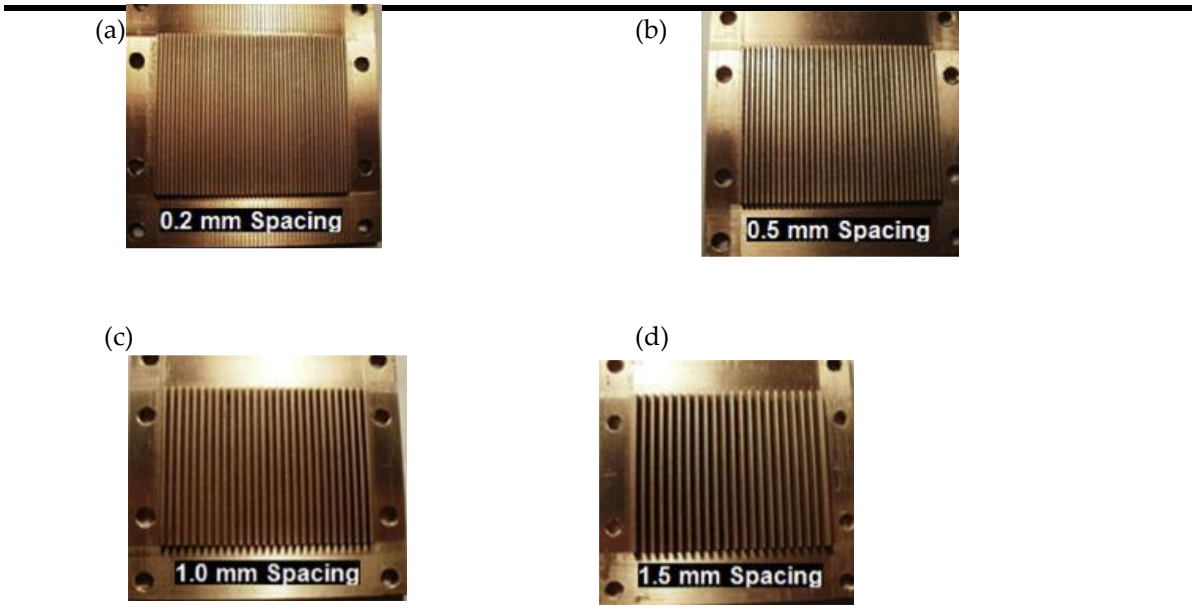

Figure 1 - Heat sinks built at different distances

Therefore, there are various geometry and methods to numerically or experimentally study heat sinks in computer equipment. Some studies indicate the optimal geometrical conditions for a particular process, while other points to varying effects of using different working fluids. However, some studies have shown how the use of other devices improves the efficiency of heat dissipation. Despite previous efforts, these analyzes still have some potential, especially for some of the heat sink geometry modifications that this present work describes it.

Thermal management is important in many sectors [8–12], such as the electronics industry [13-19], has become a development bottleneck. Many conclusions about thermal management are focused and attributed to the increased residual heat produced by Information Technology Equipment (ITE), which include devices that have a primary function related to the collection, transfer, storage, or processing of data [20]. Data Centers (DCs) represent the medium main of today digital world, housing large clusters of interconnected ITE. Thus, the demand for DC services has increased exponentially. In addition, the expected applications of artificial intelligence promise further growth in demand [21]. Consequently, the consumption of DC power has increased significantly. DCs are notoriously energy intensive buildings. DC consumption accounts for about 1.3% of the total electricity consumption worldwide [22] and its cooling systems account for 30-50% of the total electricity consumption [23]

2. Materials and Methods

The open channel design, consist in a duct in which the liquid flows with a surface subjected to atmospheric pressure and the flow is assumed fully developed at the channel inlet.

Figure 2 (a) shows the inlet velocity, V_{in}, height of the fins, H, heat flow to the bottom is applied, distance between the tip of the fins and the roof of the channel, L, height of base of heat sink model, B, the temperature of the base of heat sink, T_b. Deflectors element are placed between

Preprints (www.preprints.org) | NOT PEER-REVIEWED | Posted: 6 June 2023 doi:10.20944/preprints202306.0457.v1

rectangular fin profile for all configurations of this study. Top view in Figure 2 (b) is showed, also the arrangement and position of the deflector elements, in addition to fin spacing, b, S_T and S_L are transversal and longitudinal pitch respectively, finally a represent the fin side length. The channel walls are immovable. Figure 2 (c) shows the top view of the open channel design in a staggered arrangement for rectangular fin profile and the deflectors implemented. The shapes of the deflectors implemented in the heat sink model are presented schematically in Figure 2 (d), Figure 2(e) is a 3D view of the heat sink model, Figures 2 (f) and (g) show a view 3D model lateral and frontal respectively of the heat sink with increased size deflector in the flow direction and finally, the Figures 2 (h) and (i) show a view 3D model lateral and frontal respectively of the heat sink with decreased size deflector in the flow direction. Each parameter was based on the thermal most performance and total assessment of the system to remove heat.

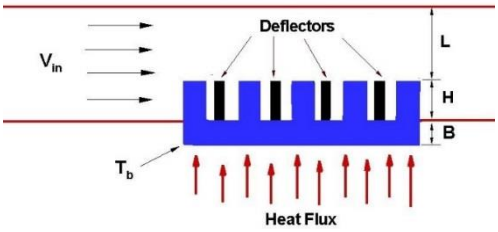

Figure 2 (a)

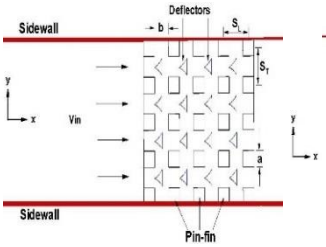

Figure 2 (b)

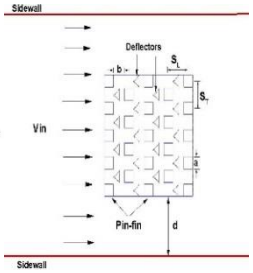

Figure 2 (c)

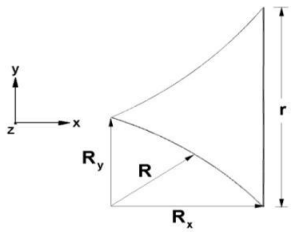

Figure 2 (d)

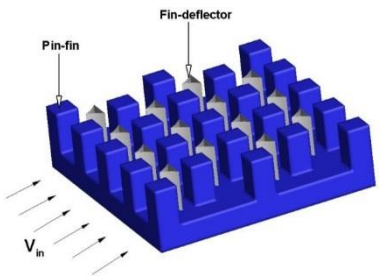

Figure 1 (e)

Preprints (www.preprints.org) | NOT PEER-REVIEWED | Posted: 6 June 2023 doi:10.20944/preprints202306.0457.v1

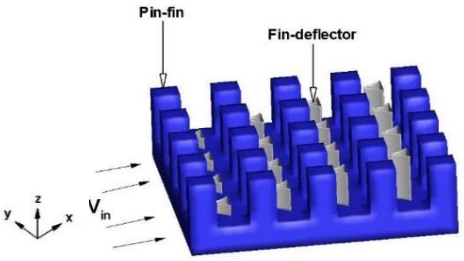

Figure 2 (f)

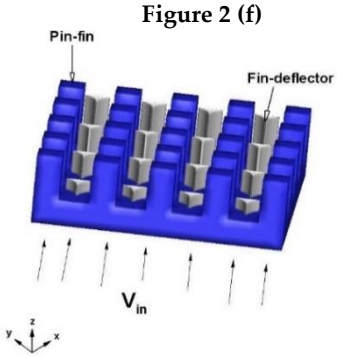

Figure 2 (g)

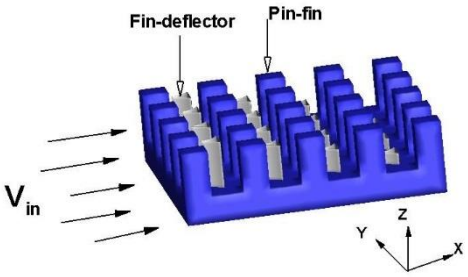

Figure 2 (h)

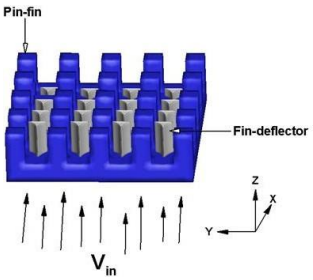

Figure 2 (i)

Figure 2. Illustration of the heat sink geometry analyzed: (a) side view with a top by-pass channel design, (b) top view of the closed channel design in arrangement aligned of deflectors implemented, (c) top view of the open channel design in arrangement of staggered deflectors collocated,(d) shape of deflector implemented, (e) 3D view of the heat sink model, (f) and (g) views 3D lateral and frontal respectively of the heat sink model with size increased deflector, (h) and (i) view 3D lateral and frontal respectively of the heat sink model with size decreased deflector. At the same time, the size of the rectangular fin profile, remained unchanged. The dimensions that were used in the analysis are shown in Table 1. These are the optimal parameters were studied in the technical literature [24].

Preprints (www.preprints.org) | NOT PEER-REVIEWED | Posted: 6 June 2023 doi:10.20944/preprints202306.0457.v1

Table 1. Dimensions and configurations of the pin-fin heat sink model and positions of deflectors implemented in the model.

Parameter [mm]	5x5 fin configurations aligned in staggered arrangements	8x8 fin configurations aligned in staggered arrangements
a	2.5	1.5
b	3.13	1.86
B	2.5	2.5
C	25	25
d	12.5	12.5
e	1.125, 2.25, 3.375, 4.5	0.642, 1.284, 1.926, 2.568, 3.21, 3.852, 4.5
H	4.5	4.5
L	0, 2.25, 4.5, 6.75, 9, 11.25, 13.5	0, 2.25, 4.5, 6.75, 9, 11.25, 13.5
P_L	2.252	2.24
R	1.22	0.65
R	2.24	1.2
R_x	1.68	0.9
R_y	1.12	0.6

Open channel

To create the *by-pass effect* in the channel design, on top and sides of the heat sink finned, it not restricted to that the entire amount of flow to circulate through of the heat sink model. Figure 3 shows the described it.

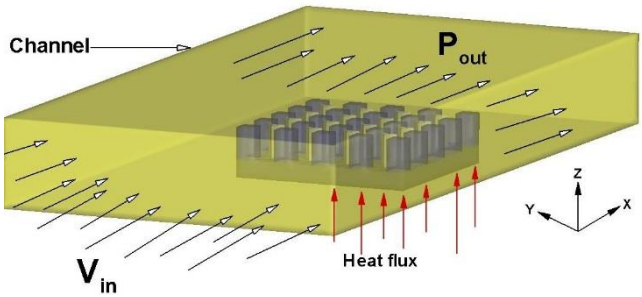

Figure 3. View 3D for an open channel design.

Closed channel

The top and the floor of the channel design show that on the heat sink model, there is not space created (*by-pas effects*) through which the flow passes freely, thereby forcing the flow to pass completely through the deflectors implemented and the heat sink model. Figure 4 shows the described.

Preprints (www.preprints.org) | NOT PEER-REVIEWED | Posted: 6 June 2023 doi:10.20944/preprints202306.0457.v1

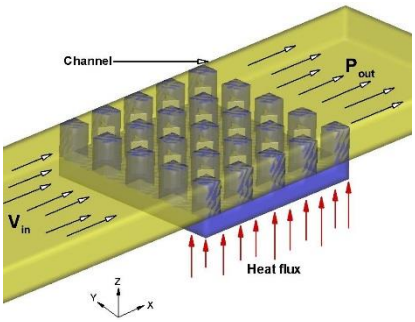

Figure 4. View 3D for a closed channel design.

2.1. Experiments Configuration Computational Analysis

A model was established. It consists of a heat sink prototype, with a base to which a heat flux Q = 8500 W/m² is applied. To avoid system, overheat a flow of air is directed about the fins of the heat sink model.

- Steady-state
- Incompressible flow
- Heat sink base, uniform heat flux, Q = 8500 W/m²
- Heat transfer by radiation is not considered
- Constant properties

2.2. Governing Equations

In the thermal problem of computational fluid dynamics, the equations governing the whole system are continuity, momentum, and energy for fluids, and only the energy formula for solids.

For computational fluid-dynamic thermal problems, the equations that govern the entire system are the Continuity, Momentum and Energy equations for the fluid, for the solid only the equation of the Energy. Equation (1) shows the simplified equation of continuity on rectangular coordinates for the fluid.

Through Equations (2)-(4) it shown the simplified coordinate momentum equations rectangular for each of the cartesian coordinates of the fluid domain.

Finally, Equations (6) indicate the simplified coordinate energy equations rectangular, for the solid and the fluid, respectively.

Preprints (www.preprints.org) | NOT PEER-REVIEWED | Posted: 6 June 2023 doi:10.20944/preprints202306.0457.v1

$$\frac{\partial u}{\partial x}+\frac{\partial v}{\partial y}+\frac{\partial w}{\partial z}=0 \quad (1)$$

$$u\frac{\partial u}{\partial x}+v\frac{\partial u}{\partial y}+w\frac{\partial u}{\partial z}=-\frac{\partial P}{\partial x}+\mu\left(\frac{\partial^2 u}{\partial x^2}+\frac{\partial^2 u}{\partial y^2}+\frac{\partial^2 u}{\partial z^2}\right) \quad (2)$$

$$u\frac{\partial v}{\partial x}+v\frac{\partial v}{\partial y}+w\frac{\partial v}{\partial z}=-\frac{\partial P}{\partial y}+\mu\left(\frac{\partial^2 v}{\partial x^2}+\frac{\partial^2 v}{\partial y^2}+\frac{\partial^2 v}{\partial z^2}\right) \quad (3)$$

$$u\frac{\partial w}{\partial x}+v\frac{\partial w}{\partial y}+w\frac{\partial w}{\partial z}=-\frac{\partial P}{\partial z}+\mu\left(\frac{\partial^2 w}{\partial x^2}+\frac{\partial^2 w}{\partial y^2}+\frac{\partial^2 w}{\partial z^2}\right) \quad (4)$$

$$\left(u\frac{\partial T}{\partial x}\right)+\left(v\frac{\partial T}{\partial y}\right)+\left(w\frac{\partial T}{\partial z}\right)=\alpha\left(\frac{\partial^2 T}{\partial x^2}+\frac{\partial^2 T}{\partial y^2}+\frac{\partial^2 T}{\partial z^2}\right) \quad (5)$$

$$\frac{\partial^2 T}{\partial x^2}+\frac{\partial^2 T}{\partial y^2}+\frac{\partial^2 T}{\partial z^2}=\frac{\rho_f c_{p,f}}{k_f}\left(u\frac{\partial T}{\partial x}+v\frac{\partial T}{\partial y}+w\frac{\partial T}{\partial z}\right) \quad (6)$$

The average Nusselt number Eq. (7), was determined as:

$$\overline{Nu}=\frac{2\bar{h}s}{k} \quad (7)$$

Where $\bar{h}$ in Eq. (8), is obtained by deduction of

$$\bar{h}=\frac{1}{A}\int h d A_s \quad (8)$$

The friction coefficient Eq. (9), was determined as:

$$f=\frac{\Delta P}{2\rho {u_{in}}^2} \quad (9)$$

Geometric parameter described are shown in Figure 5.

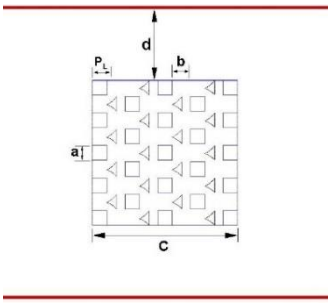

Figure 5. Geometric parameters.

Also considered:

- Air temperature at the entrance of the channel is the ambient temperature (300 K).
- A constant heat flux is supplied to the base of the heat sink model.
- Turbulent model k – ϵ (RNG).

The k – ϵ (RNG) model is implemented on renormalization of the group theory. The boundary conditions listed above are schematized in Figure 6.

Preprints (www.preprints.org) | NOT PEER-REVIEWED | Posted: 6 June 2023 doi:10.20944/preprints202306.0457.v1

The equations used in this model are like the standard k–ϵ model but with some refinements that allow its application for low and high Reynolds numbers. Solves two closure equations, for the turbulent kinetic energy (k) and other for the velocity of turbulent dissipation (ϵ).

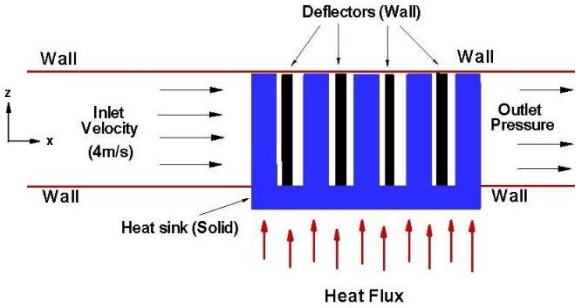

Figure 6. Scheme of the boundary conditions for computational analysis of model.

2.3. Convergence Criterion

To assure the convergence, were to set up the residuals of the equations of continuity, velocity, and $k - \epsilon$ data value of convergence of 1×10^{-3}, while for the equation energy, the residual is set to a convergence value of 1×10^{-6}.

The mesh is created by tetrahedral and triangular elements considering both solid and fluid domains, providing confidence in the results; the fluid domain is discretized in small cells or finite volume called elements that form a mesh. The density of nodes or elements change from one region to another, accumulating a greater number of them in areas where large variations are expected in some variable. It is important to know which areas expect higher gradients and to consider if a finer mesh is important to refine the mesh, such as in the contact area between the fin-deflectors implemented and fluid used in the medium suitable. The quality of the mesh largely determines the reliability of the results.

To better understand the minimization error generated by the mesh, a Mesh Sensibility Analysis is carried out. This analysis is bases of the fact of generating an "initial" mesh in the model and getting the numerical solution for the specific boundary and operating conditions. Once the solution is computed, the number of elements of the mesh is increased (the number of elements may be increased twice the number of elements used in the "initial" mesh), generating a "second" mesh. Then, the model is solved using this improved mesh considering the same boundary and operating conditions, the results for each solution are then compared and the difference is evaluated. This process is repeated until the difference can be assumed as negligible.

In this work, the "initial" mesh was formed by 320,000 tetrahedral and triangular elements (Mesh 1). An increase of two times is done in the mesh along each axial direction (x-, y- and z-axis), generating a second mesh of elements 576,000 (Mesh 2). Once the solutions were computed and compared according to the iterative process, is taken the decision of generating three subsequent meshes (Mesh 3, Mesh 4 and Mesh 5), having 980,000, 1,660,000 and 2,850,000 elements, respectively. Figure 7-8 presents the Nusselt number and global thermal resistance variations for the five meshes. The results show that the difference generated by "meshing" is negligible when Mesh 3 is used. Analyzing the curves, it is observed that the Nusselt number and global thermal resistance variations between Mesh 4 and Mesh 5 are negligible (0,05 and 0,01 K/W, respectively).

Preprints (www.preprints.org) | NOT PEER-REVIEWED | Posted: 6 June 2023 doi:10.20944/preprints202306.0457.v1

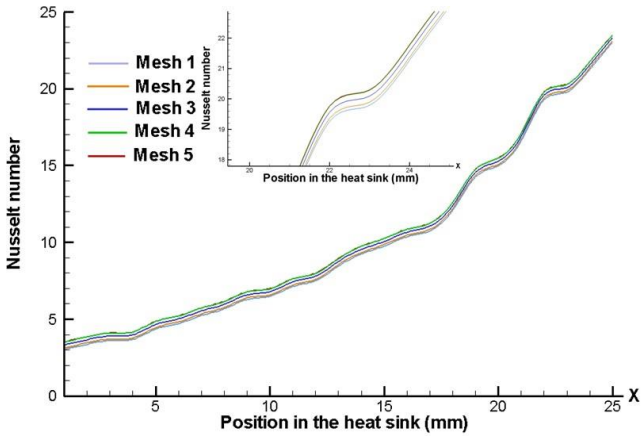

Figure 7. Mesh Sensibility Analysis for the Nusselt number

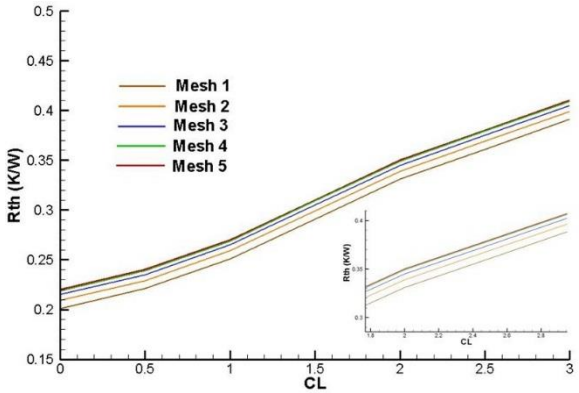

Figure 8. Mesh Sensibility Analysis for the Global thermal resistance

3. Results and Discussion

The results the simulation for the heat sink were obtained by drawing a line at the center of the heat sink and are shown in the next graphics. The accelerating flows inside the heat sink channel and the fin-deflectors implemented produces a pressure drop between the channel entrance and exit region.

Figures (9)-(12) show the pressure distribution along the duct, with an inlet velocity of 4 m/s for heat sink model in aligned and staggered configurations of 5 x 5 and 8 x 8 respectively, making a comparison between both channels (open and closed), also is shown the effect of the implementation of the deflectors inside the system. As a result expected, it is observed that the pressure is higher at the entrance of conduct the heat sink model and decreases through path downstream.

Also, the effects of the deflectors collocated for aligned and staggered configurations, both for open channel and closed channel designs are shown in Figures (9)-(12). When deflectors were used in the closed channel design, the pressure drop trough the pin-fin heat sink arrangement increases the pumping energy required to cool the heat sink model.

Preprints (www.preprints.org) | NOT PEER-REVIEWED | Posted: 6 June 2023 doi:10.20944/preprints202306.0457.v1

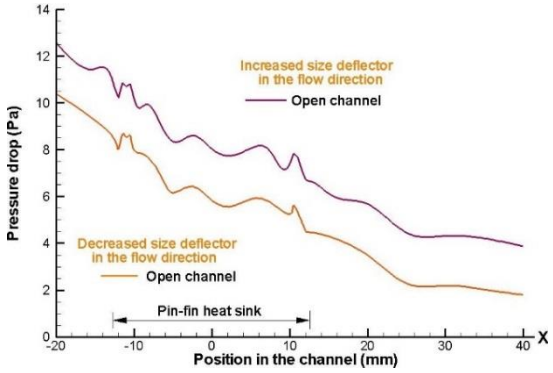

Figure 9. Effect of the deflectors implemented in open channel design on the pressure distribution along of the heat sink model, with an inlet velocity of 4 m/s, for 5 x 5 fin configurations in aligned arrangement.

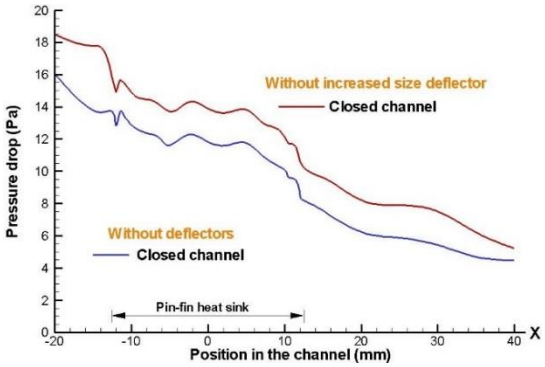

Figure 10. Effect of deflectors implemented in closed channel design on the pressure distribution along of the heat sink model, with an inlet velocity of 4 m/s, for 5 x 5 fin configurations in aligned arrangement.

The Figures (9) and (10) show that the trend is consistent increasing the size of the deflectors implemented along the heat sink model. However, has a higher pressure drop for the case that presents a closed channel and the deflectors size increase along the direction flow. This is because the airflow circulating through the heat sink model, it encounters in this path with the presence of increased resistance to flow, as well as an increase in the size of the deflectors collocated that hindering the circulation of the airflow freely.

Figures (11)-(13) show a pressure drop greater for the 5 x 5 fins configurations in aligned arrangements, as expected and for the case where the height of the deflectors implemented is kept constant, which are positioned along and within the heat sink model. A higher pressure drop is obtained when the height of deflector increases in closed channel design, due to increasing contact of airflow with deflector elements.

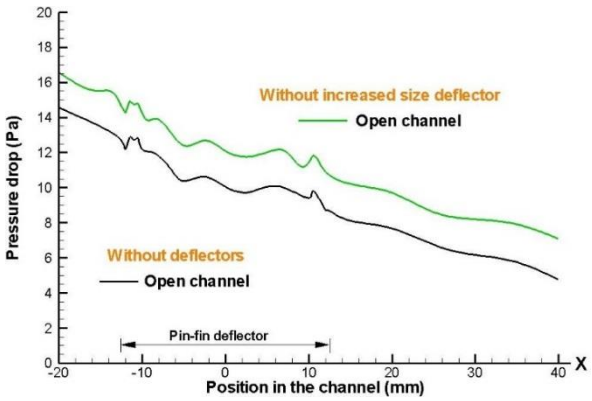

Figure 11. Effect of the deflectors implemented in open channel design on the pressure distribution along the heat sink model, with an inlet velocity of 4 m/s, for 5 x 5 fin configurations in aligned

Preprints (www.preprints.org) | NOT PEER-REVIEWED | Posted: 6 June 2023 doi:10.20944/preprints202306.0457.v1

arrangement.

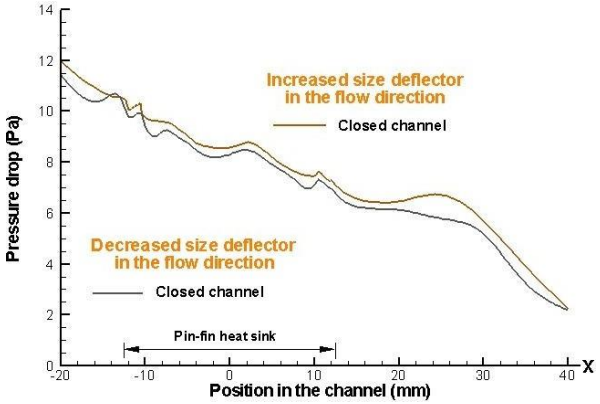

Figure 12. Effect of the deflectors implemented in closed channel design on the pressure distribution along the heat sink model, with an inlet velocity of 4 m/s, for 5 x 5 fin configurations in aligned arrangement.

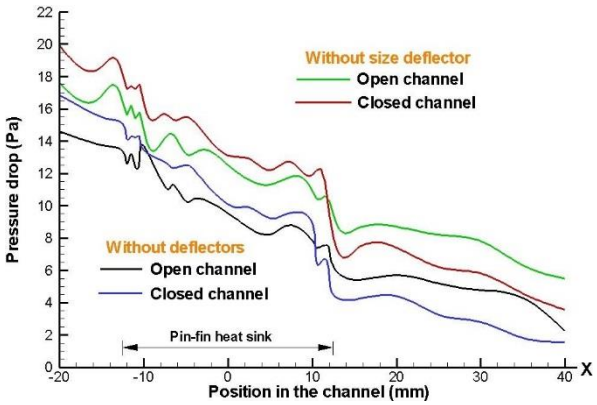

Figure 13. Effect of the deflectors implemented in open and closed channel design on the pressure distribution along the heat sink model, with an inlet velocity of 4 m/s, for 8 x 8 fin configurations in aligned arrangement.

Figures (14) show the scenario in which the size deflector increases and decreases, with height of the deflectors implemented in the flow direction, a higher-pressure drop is obtained when the height of deflector increases in closed channel design, due to enhancement contact of airflow with each deflector element of system.

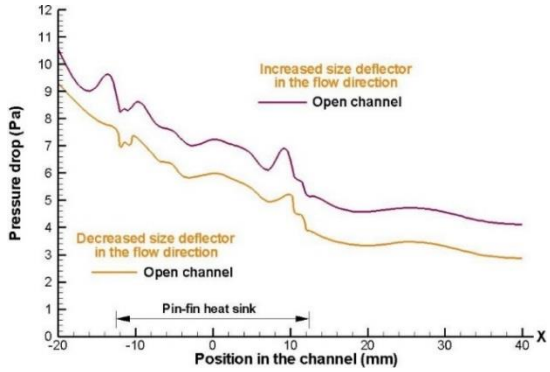

Figure 14. Effect to collocate deflectors in open channel design on pressure distribution along of heat sink model, with an inlet velocity of 4 m/s, for 5 x 5 fin configurations in staggered arrangement.

Preprints (www.preprints.org) | NOT PEER-REVIEWED | Posted: 6 June 2023 doi:10.20944/preprints202306.0457.v1

Figure 15 shows that using a staggered arrangement results in a decrease in the drop pressure for the two channel designs (open and closed). Nevertheless, when there is an open channel design, the air that supplied circulate more freely through medium, but when the flow is forced to pass entirely within the heat sink model, (which case is the closed channel design); it shows a greater pressure drop, due to the presence of the deflectors inside the heat sink model).

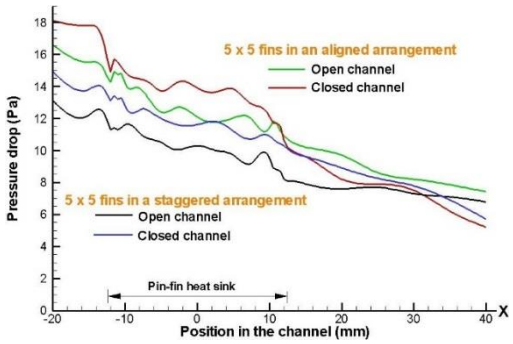

Figure 15. Effect of deflectors implemented in closed channel design on the pressure distribution along of the heat sink model, with an inlet velocity of 4 m/s, for 5 x 5 fin configurations in a staggered arrangement.

Figure 16 shows a higher drop pressure for the case that increased size deflector implemented. The increase in drop pressure a cross the heat sink inlet, is due to the strangulation of air flow to reach the fins and begin contact with each deflector element of system.

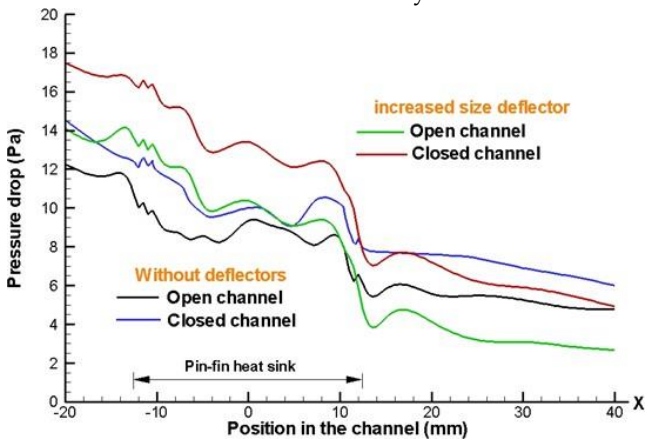

Figure 16. Effect to collocate deflectors in open and closed channel designs on the pressure distribution along of the heat sink model, with an inlet velocity of 4 m/s, for 8 x 8 fin configurations in a staggered arrangement.

Figure 17, shows that the pressure drop for different rates clearance (CL), presents a similar behavior in the experimental and numerical cases, this is due a that the pressure drop decreases over the distance created on the upper heat sink model (by-pass). For effect by-pass in the drop pressure, the pressure drop is lower, because to that the amount of flow passing by the fins is reduced. The pressure drop measured is acceptable, according to the predicted values and the increasing contraction and expansion pressure losses at the channel designs (inlet and outlet). In general, the total heat sink model pressure drop depends on four major factors: the friction factors, the heat sink geometry, the velocities approach and of the air within channel respectively.

Preprints (www.preprints.org) | NOT PEER-REVIEWED | Posted: 6 June 2023 doi:10.20944/preprints202306.0457.v1

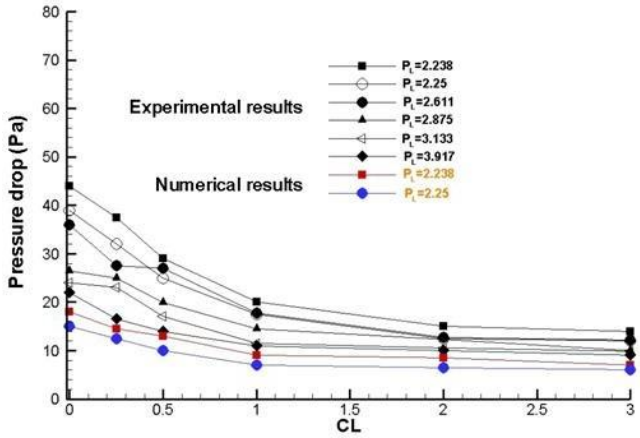

Figure 17. Experimental and numerical results [5] without deflectors element collocated for total pressure drop vs different rate clearance (CL) with an inlet velocity of 4 m/s and different PL´s, with H=22.5 mm and H=4.5 mm

Figures (18) and (19) show the effect which occurs at admit in the Nusselt number, increase and decrease the height of the deflectors element, presenting a higher heat removal for the 8 x 8 fins in a staggered arrangement, in both staggered arrangement the heat removal is higher by about 6% when there is an increase in the height of the deflectors in the air flow direction. It is also noted that the graphics intersect in certain areas of the heat sink models, this is because to that in these areas the size of the deflectors is approximately similar for both cases.

Clearly the value of the Nusselt number increases along the heat sink model; this is mainly caused by the acceleration of the fluid that is leaving the pin-fin and the section of deflector elements and also by the instability that is generated when the air is passing through. These results are obtained via the numerical results.

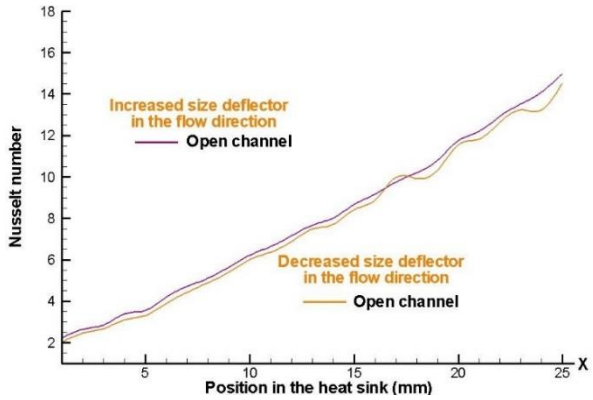

Figure 18. Local Nusselt number with an inlet velocity of 4 m/s, for a 8 x 8 fin configurations in staggered arrangement.

Preprints (www.preprints.org) | NOT PEER-REVIEWED | Posted: 6 June 2023 doi:10.20944/preprints202306.0457.v1

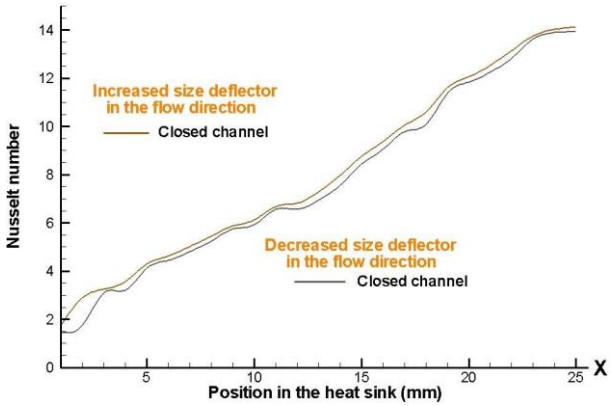

Figure 19. Local Nusselt number with an inlet velocity of 4 m/s, for a 5x 5 fin configurations in staggered arrangement.

Figure 20 shows a comparison, in the when for both arrangement is greater heat dissipation for a closed channel design. However, the greater heat dissipation is presents for the cases of aligned arrangements. The 5 x 5 fin configurations in staggered arrangement, presents less wetted area, because this arrangement has fewer fins and thus less conduct area, decreasing the efficiency of the heat sink model.

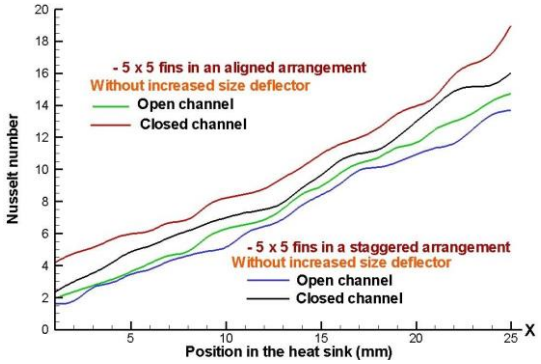

Figure 20. Comparison of local Nusselt number for 5 x 5 fin configuration in aligned and staggered arrangements along of the heat sink model, with an inlet velocity of 4 m/s.

It must be remembered that in an open channel there will be free flow on the sides of the dissipator, and for a closed channel design, the flow is forced to circulate through the elements deflector and inside the heat sink model, thus achieving an increase in the Nusselt number.

Figures (21) and (22) shown comparisons of the local Nusselt number with and without deflector elements, for both aligned arrangements and closed channel design for a rate clearance, CL=0.

Thus, by using deflector elements there is clearly an increase of the local Nusselt number; this is due to the acceleration of the fluid caused by the deflector, and to the fact that the flow is being directed towards areas that otherwise will have stagnation of the airflow; the largest local Nusselt number appears at the end of the pin-fin heat sink model. At the entrance of the pin-fin arrangement the Nusselt number is the same for both cases, and it has a higher increment through the heat sink model when the deflector elements are used in an aligned configuration.

Preprints (www.preprints.org) | NOT PEER-REVIEWED | Posted: 6 June 2023 doi:10.20944/preprints202306.0457.v1

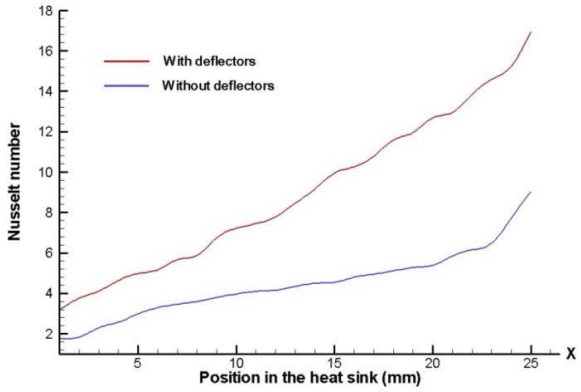

Figure 21. Effect of the deflector elements on the Nusselt number along the position in the heat sink model, with an inlet velocity of 4 m/s, for a 5 x 5 fin configuration in aligned arrangement.

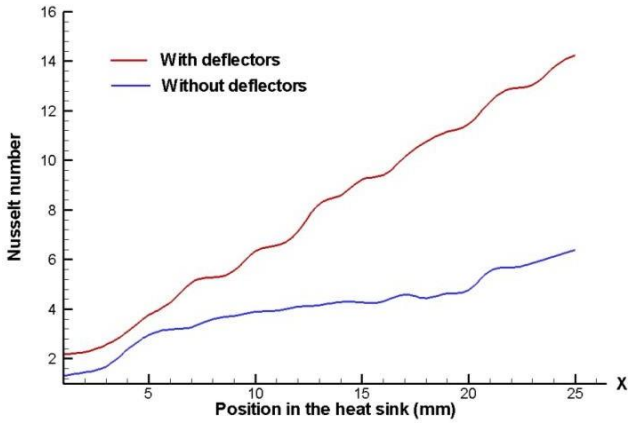

Figure 22. Effect of the deflector elements on the Nusselt number along the position in the heat sink model, with an inlet velocity of 4 m/s, for a 8 x 8 fin configuration in aligned arrangement.

It is clear that the Nusselt number improves with the presence of deflector elements for both pin-fin heat sinks arrangements (aligned and staggered), but the Nusselt number is larger when there is an 8 x 8 fin configuration and the channel design is closed.

Figures (23) and (24) show that comparison between arrangements aligned and staggered, it is presents that the thermal resistance is higher for the staggered arrangement, this means that in these types of arrangements the heat removal is lower.

Preprints (www.preprints.org) | NOT PEER-REVIEWED | Posted: 6 June 2023 doi:10.20944/preprints202306.0457.v1

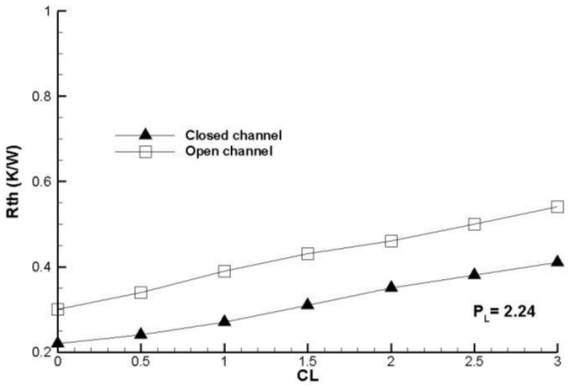

Figure 23. Global thermal resistance with different rate clearance, for 8 x 8 fin configurations and deflectors collocated in a staggered arrangement.

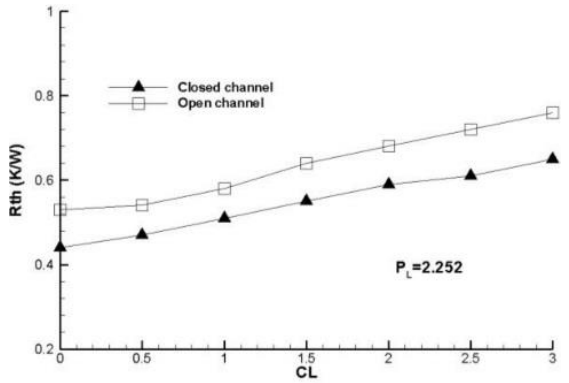

Figure 24. Global thermal resistance with different rate clearance, for 5 x 5 fin configuration and deflectors collocated in a staggered arrangement.

It is expected that the global thermal resistance increases according to the rate clearance is higher, this is due to the fact that a fraction of the air goes to the top of the fins (bypass); this is also greater when the distance between the fins is greater. The thermal resistance increases according the rate clearance is increased, as well as a lower thermal resistance is presents for the case 8 x 8 fins arrangement because this provides the most amount wetted area.

The amount minor of wetted area is shown is the 5 x 5 fins arrangement and the configuration that present a fewer global thermal resistance is the 8 x 8 fins arrangement, because to that is present a smaller spacing between fins.

Figure 25 shows experimental and numerical results that the thermal resistance tends to increase as a function of the clearance ratio (CL), as expected. It also has a lower thermal resistance for case where decreases the height of the fin which is the numerical case.

This leads to the conclusion that global thermal resistance increases with decreasing wetted area of the fins, or to decrease the convection coefficient and is a consequence of having fewer wetted area of the fins in the heat sink.

Preprints (www.preprints.org) | NOT PEER-REVIEWED | Posted: 6 June 2023 doi:10.20944/preprints202306.0457.v1

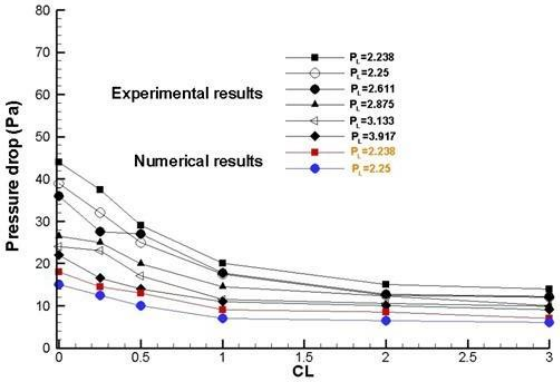

Figure 25. Numerical results for thermal resistance vs clearance (CL) for H=22.5 mm, H = 4.5 mm and an inlet velocity of 4 m/s, in a closed channel design.

Figures (26) and (27) show that for both cases the thermal resistance results lower for the aligned arrangements of 8 x 8 fins, for both cases in closed channel design. The close channel was designed with the target that the by-pass effect is not present at the top and the sides of the heat sink, in order to force the entire air flow to pass through the deflector elements placed within of heat sink finned and thereby is present a higher heat removal.

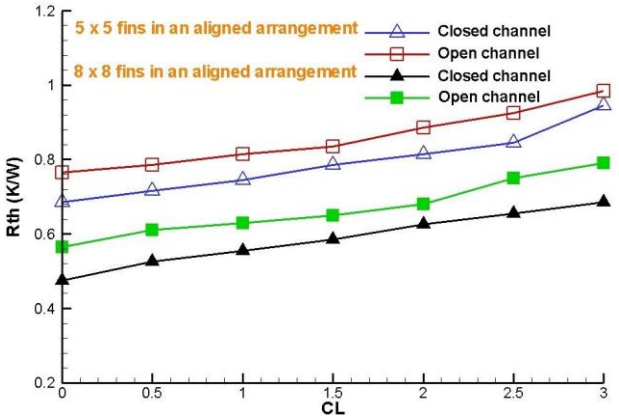

Figure 26. Comparison global thermal resistance for different clearance ratio, decreased size deflector in the air

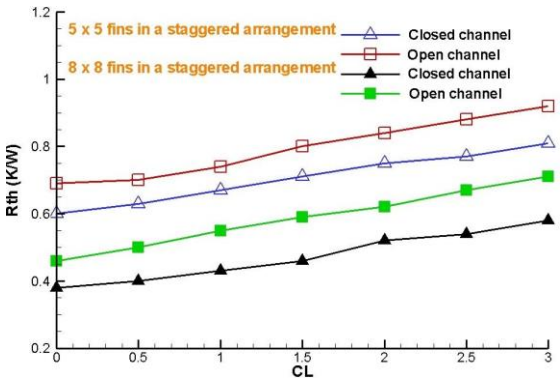

flow direction for both arrangements.

Figure 27. Comparison global thermal resistance for different clearance ratio, decreased size deflector in the air flow direction for both cases.

Preprints (www.preprints.org) | NOT PEER-REVIEWED | Posted: 6 June 2023 doi:10.20944/preprints202306.0457.v1

4. Conclusion

This analysis confirms a thermal management solution as a result of the urgent need to enhance the influence of the deflectors on the pressure drop behavior of the Nusselt number. Deflectors implemented clearly help prevent stagnation, which reduces heat. It is concluded that when the closed channel design is used, it helps to improve the Nusselt number. However, at a given heat flux, it affects the amount of energy removed. Accordingly, it is necessary to continue this study to optimize the flow and geometric parameters; conceivably a second law-based analysis (such as minimum entropy generation analysis) provides optimal operating conditions. A study is needed to optimize the flow and geometric parameters and the new fin configurations; perhaps a second law-based analysis (such as the minimum entropy generation analysis) will provide the optimum operating conditions. Finally, to determine the most efficient fin profile in terms of maximum heat loss and fin efficiency (decrease the weight of the prototype heat sink and increase heat removal).

Nomenclature

A_s wetted area of the pins, m^2
a fin side (rectangular fin profile), mm
b distance between two fins in the air flow direction, mm
B height of base heat sink model, mm
C width heat sink model, mm
CL clearance ratio, L/H
c_p specific heat, J/kgK
d_f fin hydraulic diameter, mm
d distance between heat sink and the walls, mm
e increase height or reduce from deflector along flow direction
f friction coefficient
H fin height, mm
average heat transfer coefficient, $W/(m^2K)$
h heat transfer coefficient, $W/(m^2K)$
L height of the top by – pass section (top clearance), mm
P_L reference non-dimensional longitudinal pitch, S_L/d_f
P_T reference non-dimensional longitudinal pitch, S_T/d_f
n number of rows or columns
Nu Nusselt number
Q Heat flux, W/m^2
R radius of the deflector element, mm
r deflectors side, mm
R_x position of the deflector in the X-rectangular coordinate, mm
R_y position of the deflector in the Y-rectangular coordinate, mm
Re Reynolds number
R_{th} global thermal resistance K/W
S_L longitudinal pitch, mm
S_T transversal pitch, mm
V_{in} inlet velocity, m/s

Greek symbols

ΔP pressure drop in the finned section, Pa density, kg/m^3

 doi:10.20944/preprints202306.0457.v1

Acknowledgment: To all the people and academic institutions that made this work possible, especially to Instituto Politecnico Nacional and CONACYT for the financing my studies.

References

[1] Wu W, Wang S, Wu W, Chen K, Hong S, Lai Y. A critical review of battery thermal performance and liquid-based battery thermal management. Energy Conversion Manag ement 2019; 182:262–81. January.

[2] Shi X, Pan J, Wang H, Cai H. Battery electric vehicles: what is the minimum range required? Energy 2018; 166:352–8.

[3] Han D, et al. Orthogonal experimental design of liquid-cooling structure on the cooling effect of a liquid-cooled battery thermal management system. Appl Therm Eng 2017; 132:508–20.

[4] Regulated extra low voltage power supplies for detector electronics. CERN LHC IT-3330/PH/EXP Technical Specification; 2004.

[5] J. Ramirez Vazquez, A. Hernandez Guerrero, J. Zuñiga Cerroblanco, J. Rubio-Arana Implementations of Deflectors to Improve the Performance of Heat Sinks. Conference Engineering Systems Design and Analysis. American Society of Mechanical Engineers; 44854: 693-6982012.

[6] Hamdi E. Ahmed, B.H. Salman, A.Sh. Kherbeet, M.I. Ahmed, Optimization of thermal design of heat sinks: A review, International Journal of Heat and Mass Transfer 118 (2018) 129–153. doi: 10.1016/j.ijheatmasstransfer.2017.10.099.

[7] Saad Ayub Jajja, Wajahat Ali, Hafiz Muhammad Ali, Aysha Maryam Ali, Water cooled minichannel heat sinks for microprocessor cooling: Effect of fin spacing, Applied Thermal Engineering 64 (2014) 76-82. doi: 10.1016/j.applthermaleng.2013.12.007.

[8] U. Zeynep Uras, M. Arık, E. Tamdogan, Thermal performance of a light emitting diode light engine for a multipurpose automotive exterior lighting system with competing board technologies, J. Electron. Packag. 139 (2) (2017) 020907 (8 pages).

[9] U.Z. Uras, E. Tamdogan, M. Arık, Thermal enhancement of an LED light engine for automotive exterior lighting with advanced heat spreader technology, in: Proceedings of the ASME International Mechanical Engineering Congress and Exposition, American Society of Mechanical Engineers, 2016 V010T013A050.

[10] A .M. Abubaker, A .D. Ahmad, A .A. Salaimeh, N.K. Akafuah, K. Saito, A novel solar combined cycle integration: an exergy-based optimization using artificial neural network, Renew. Energy 181 (2021) 914–932.

[11] L. Al-Ghussain, A. Darwish Ahmad, A.M. Abubaker, M.A. Hassan, Technoeconomic feasibility of thermal storage systems for the transition to 100% renewable grids, Available at SSRN 3916215. 2021.

[12] A .D. Ahmad, A .M. Abubaker, Y.S. Najjar , Y.M.A. Manaserh , Power boosting of a combined cycle power plant in Jordan: an integration of hybrid inlet cooling & solar systems, Energy Convers. Manag. 214 (2020) 112894.

[13] M. Bahiraei, S. Heshmatian, Electronics cooling with nanofluids: a critical review, Energy Convers. Manag. 172 (2018) 438–456.

[14] J. Li, L. Lv, G. Zhou , X. Li , Mechanism of a microscale flat plate heat pipe with extremely high nominal thermal conductivity for cooling high-end smartphone chips, Energy Convers. Manag. 201 (2019) 112202.

[15] C.H. Hoang, S. Rangarajan, Y. Manaserh, M. Tradat, G. Mohsenian , L. Choobineh , A. Ortega, S. Schiffres, B. Sammakia, A review of recent developments in pumped two-phase cooling technologies for electronic devices, IEEE Trans. Compon. Packag. Manuf. Technol. 11 (2021) 1565–1582.

[16] C. Caceres, A. Ortega , A. Wemhoff, G.F. Jones, Numerical analysis of two phase cross-flow heat exchanger for high power density equipment in data centers under dynamic conditions, in: Proceedings of the 19th IEEE Intersociety Conference on Thermal and Thermomechanical Phenomena in Electronic Systems (ITherm), IEEE, 2020, pp. 520–529.

 doi:10.20944/preprints202306.0457.v1

[17] C. Caceres, A. Ortega , L. Silva-Llanca, G.F. Jones , N. Sapia, Thermal and exergy analysis in UPS and battery rooms by numerical simulations, in: Proceedings of the 17th IEEE Intersociety Conference on Thermal and Thermomechanical Phenomena in Electronic Systems (ITherm), IEEE, 2018, pp. 521–529.

[18] R. Gupta , S. Asgari, H. Moazamigoodarzi, D.G. Down , I.K. Puri, Energy, exergy and computing efficiency based data center workload and cooling management, Appl. Energy 299 (2021) 117050 .

[19] X. Yuan, X. Zhou, Y. Pan, R. Kosonen, H. Cai, Y. Gao, Y. Wang, Phase change cooling in data centers: a review, Energy Build. 236 (2021) 110764.

[20] X. Gong, Z. Zhang, S. Gan, B. Niu, L. Yang , H. Xu, M. Gao, A review on evaluation metrics of thermal performance in data centers, Build. Environ. 177 (2020) 106907.

[21] W.X. Chu, C.S. Hsu, Y.Y. Tsui, C.C. Wang, Experimental investigation on thermal management for small container data center, J. Build. Eng. 21 (2019) 317–327.

[22] C.S. Sharma, M.K. Tiwari, S. Zimmermann, T. Brunschwiler, G. Schlottig, B. Michel, D. Poulikakos, Energy efficient hotspot-targeted embedded liquid cooling of electronics, Appl. Energy 138 (2015) 414–422.

[23] Y. Ma, G. Ma , S. Zhang , S. Xu , Experimental investigation on a novel integrated system of vapor compression and pump-driven two phase loop for energy saving in data centers cooling, Energy Convers. Manag. 106 (2015) 194–200.

[24] L. Luviano Ortiz, A. Hernandez-Guerrero, C. Rubio Arana, R. Romero-Mendez, Heat transfer enhancement in a horizontal channel by the addition of curved deflectors, International Journal of Heat and Mass Transfer, 51 (2008)3972-3984.